

THE FIRST SURVEY OF X-RAY FLARES FROM GAMMA-RAY BURSTS OBSERVED BY *SWIFT*: TEMPORAL PROPERTIES AND MORPHOLOGY

G. CHINCARINI,^{1,2} A. MORETTI,¹ P. ROMANO,^{1,2} A. D. FALCONE,³ D. MORRIS,³ J. RACUSIN,³ S. CAMPANA,¹ S. COVINO,¹
C. GUIDORZI,^{1,2} G. TAGLIAFERRI,¹ D. N. BURROWS,³ C. PAGANI,³ M. STROH,³ D. GRUPE,³ M. CAPALBI,⁴ G. CUSUMANO,⁵
N. GEHRELS,⁶ P. GIOMMI,⁴ V. LA PAROLA,⁵ V. MANGANO,⁵ T. MINEO,⁵ J. A. NOUSEK,³ P. T. O'BRIEN,⁷
K. L. PAGE,⁷ M. PERRI,⁴ E. TROJA,⁵ R. WILLINGALE,⁷ AND B. ZHANG⁸

Received 2007 February 14; accepted 2007 July 6

ABSTRACT

We present the first systematic investigation of the morphological and timing properties of flares in GRBs observed by *Swift* XRT. We consider a large sample drawn from all GRBs detected by *Swift*, *INTEGRAL*, and *HETE-2* prior to 2006 January 31, which had an XRT follow-up and which showed significant flaring. Our sample of 33 GRBs includes long and short, at low and high redshift, and a total of 69 flares. The strongest flares occur in the early phases, with a clear anticorrelation between the flare peak intensity and the flare time of occurrence. Fitting each X-ray flare with a Gaussian model, we find that the mean ratio of the width and peak time is $\langle \Delta t/t \rangle = 0.13 \pm 0.10$, albeit with a large scatter. Late flares at times >2000 s have long durations, $\Delta t > 300$ s, and can be very energetic compared to the underlying continuum. We further investigated whether there is a clear link between the number of pulses detected in the prompt phase by BAT and the number of X-ray flares detected by XRT, finding no correlation. However, we find that the distribution of intensity ratios between successive BAT prompt pulses and that between successive XRT flares is the same, an indication of a common origin for gamma-ray pulses and X-ray flares. All evidence indicates that flares are indeed related to the workings of the central engine and, in the standard fireball scenario, originate from internal shocks rather than external shocks. While all flares can be explained by long-lasting engine activity, 29/69 flares may also be explained by refreshed shocks. However, 10 can *only* be explained by prolonged activity of the central engine.

Subject headings: gamma rays: bursts — X-rays: bursts

Online material: color figures

1. INTRODUCTION

The advent of *Swift* (Gehrels et al. 2004) has brought substantial advances in our knowledge of GRBs, including the discovery of the first afterglow (with a position known to several arcseconds precision) of a short burst. *Swift* also brought on the definition of a possible third class of GRBs (Gehrels et al. 2006), the discovery of a smooth transition between prompt and afterglow emission (Tagliaferri et al. 2005; Vaughan et al. 2006; O'Brien et al. 2006), and the definition of a canonical X-ray light curve (Nousek et al. 2006; O'Brien et al. 2006; Zhang et al. 2006). The latter includes a steep early part ($\propto t^{-\alpha_1}$ with $3 \lesssim \alpha_1 \lesssim 5$, typically interpreted as GRB high-latitude emission), a flat phase ($0.5 \lesssim \alpha_2 \lesssim 1$, generally interpreted as due to energy injection into the external shock), and a last, steeper part ($1 \lesssim \alpha_3 \lesssim 1.5$, the only one observed by pre-*Swift* X-ray instruments), with the predicted t^{-1} decay. Sometimes, a further steepening is detected after the normal decay phase, which is consistent with a jet break (Zhang et al. 2006).

What may be the most surprising discovery is the presence of flares in a large percentage of X-ray light curves. Flares had been previously observed in GRB 970508 (Piro et al. 1999), GRB 011121, and GRB 011211 (Piro et al. 2005). Piro et al. (2005)

suggested that the X-ray flares observed in the latter two events were due to the onset of the afterglow, since the spectral parameters of these flares were consistent with those of their afterglow. Starting from XRF 050406 (Burrows et al. 2005b; Romano et al. 2006b), GRB 050502B (Falcone et al. 2006), and GRB 050607 (Pagani et al. 2006), we have learned that flares can be considerably energetic and that they are often characterized by large flux variations. Indeed, the flare fluences can be up to 100% of the prompt fluence and the flare fluxes, measured with respect to the underlying continuum, $\Delta F/F$, can vary in very short timescales $\Delta t/t_{\text{peak}}$ ($\Delta F/F \sim 6, 500$ and 25 , $\Delta t/t_{\text{peak}} \ll 1, \sim 1, \sim 1$ in XRF 050406, GRB 050502B, and GRB 050607, respectively, where Δt measures the duration of the flare and t_{peak} is measured with respect to the trigger time). Furthermore, detailed spectral analysis has proven that these flares are spectrally harder than the underlying continuum (Burrows et al. 2005b; Romano et al. 2006b; Falcone et al. 2006). In particular, they follow a hard-to-soft evolution, which is reminiscent of the prompt emission (e.g., Ford et al. 1995). The spectra of the flares in GRB 050502B (Falcone et al. 2006) are better fit by a Band function (Band et al. 1993; which is the standard fitting model for GRB prompt emission) than by an absorbed power law (which usually suffices for a standard afterglow). Very often multiple flares are observed in the same light curve, with an underlying afterglow consistent with having the same slope before and after the flare. Finally, GRB 050724 (Barthelmy et al. 2005f; Campana et al. 2006) and GRB 050904 (Cusumano et al. 2006) have demonstrated that flares happen in short GRBs as well as long ones, at low and very high redshift (the record being held by GRB 050904 at $z = 6.29$).

The picture that the early detections of flares have drawn was described by Burrows et al. (2006) and Chincarini et al. (2006) and references therein, and a few conclusions were derived, albeit

¹ INAF–Osservatorio Astronomico di Brera, I-23807 Merate (LC), Italy.
² Università degli Studi di Milano, Bicocca, I-20126 Milano, Italy.
³ Department of Astronomy and Astrophysics, Pennsylvania State University, University Park, PA 16802.
⁴ ASI Science Data Center, I-00044 Frascati, Italy.
⁵ INAF–Istituto di Fisica Spaziale e Fisica Cosmica, Sezione di Palermo, I-90146 Palermo, Italy.
⁶ NASA Goddard Space Flight Center, Greenbelt, MD 20711.
⁷ Department of Physics and Astronomy, University of Leicester, Leicester, LE1 7RH, UK.
⁸ Department of Physics, University of Nevada, Las Vegas, NV 89154-4002.

based on a small sample of objects. The presence of an underlying continuum consistent with the same slope before and after the flare (GRB 050406, GRB 050502B) seems to rule out external-shock models, since no trace of an energy injection can be found; the large observed $\Delta F/F$ cannot be produced by synchrotron self-Compton in the reverse shocks; the very short timescales ($\Delta t/t_{\text{peak}} < 1$) also generally rule out external shocks, unless very carefully balanced conditions are met (e.g., Kobayashi et al. 2007); furthermore, the flare spectral properties (harder than the underlying afterglow, evolving from hard to soft) indicate a different physical mechanism from the afterglow, possibly the same as the prompt one.

In this work we present the first comprehensive temporal analysis of all GRBs observed by the X-ray Telescope (XRT; Burrows et al. 2005a)—both long and short, independently of whether they are GRBs, X-ray rich GRBs (XRRs) or X-ray flashes (XRFs; Heise et al. 2001) at low and high redshift—that showed flares in their X-ray light curves. We assess whether the evidence for prolonged engine activity accumulated on the first observed flares survives statistical investigation and discuss the case that flares are indeed related to the workings of the central engine. We also present the results of a cross-check analysis between X-ray flares and pulses detected by the Burst Alert Telescope (BAT; Barthelmy et al. 2005e) in the gamma-ray prompt emission. A second paper (Falcone et al. 2007) studies the same sample from the spectroscopic point of view, in a natural complement to this work.

This paper is organized as follows. In § 2 we describe our GRB sample, and in § 3 the data reduction procedure; in § 4 we describe our XRT data analysis, and in § 5 our cross-check analysis between X-ray flares and pulses detected by BAT in the gamma-ray prompt emission. In § 6 we present our main results, and in § 7 we discuss our findings. Throughout this paper the quoted uncertainties are given at 90% confidence level for one interesting parameter (i.e., $\Delta\chi^2 = 2.71$) unless otherwise stated. Times are referred to the BAT trigger T_0 , $t = T - T_0$, unless otherwise specified. The decay and spectral indices are parameterized as $F(\nu, t) \propto t^{-\alpha}\nu^{-\beta}$, where F_ν (ergs cm⁻² s⁻¹ Hz⁻¹) is the monochromatic flux as a function of time t and frequency ν ; we also use $\Gamma = \beta + 1$ as the photon index, $N(E) \propto E^{-\Gamma}$ (photons keV⁻¹ cm⁻² s⁻¹).

2. SAMPLE DEFINITION

We considered all GRBs detected by *Swift*, *INTEGRAL*, and *HETE-2* between the *Swift* launch and 2006 January 31 (119 events) for which XRT obtained a position (99). We then examined all light curves, searching for deviations from a power-law decay with typical breaks (hereafter the underlying power-law continuum) and excluded all light curves for which no large-scale deviations were found. We defer a detailed analysis of small-scale and small-frequency deviations, sometimes referred to as “flickering,” to a later paper.

None of the *INTEGRAL*- or *HETE-2*-triggered bursts showed any flares, although we note that these bursts were observed by XRT much later than the *Swift*-triggered ones. As we discuss in § 4.4, where we investigate the sample biases in depth, we evaluate the completeness of our sample with a large set of simulations. We established that our flare sample can be considered complete with respect to faint flares only at late times (typically 10³ s after the trigger). In Table 1 we list all the GRBs that were selected for the analysis, along with their redshifts (when available, i.e., for nine of them), T_{90} 's, and BAT fluences. This is what we refer to as our “full” sample, consisting of 33 GRBs, on which we attempted the timing analysis described in § 4. The light curves of the full sample are shown in Figure 1.

Some light curves, however, were not fit for the full analysis. For instance, although joint analysis of BAT and XRT data on

GRB 050219A (Goad et al. 2006) showed a simultaneous flare (hence its inclusion in our sample), the portion of the flare that was observed with XRT was not long enough to fully characterize it. In the same manner, a handful of events (GRB 050826, GRB 051016B, and GRB 060109), which are included in our full sample because they showed either low-signal late-time flares or a flattening in the XRT light curve, were excluded from a full analysis because of the low statistics obtained. All these special cases are marked by an asterisk in Table 1. After these exclusions, we defined our “restricted” sample, which consists of 30 GRBs on which we succeeded in performing our full analysis.

We note that our restricted sample differs from the one of Falcone et al. (2007) because of different requirements for the analysis. As an example, for GRB 050820A Falcone et al. (2007) could perform detailed spectroscopic analysis of the flare portion observed by XRT, but our full timing analysis was not applicable.

3. DATA REDUCTION

The XRT data were first processed by the *Swift* Data Center at the NASA Goddard Space Flight Center (GSFC) into level 1 products (event lists). Then they were further processed with the XRTDAS (ver. 1.7.1) software package, written by the ASI Science Data Center (ASDC) and distributed within FTOOLS to produce the final cleaned event lists. In particular, we ran the task `xrtpipeline` (ver. 0.9.9) applying calibration and standard filtering and screening criteria. An on-board event threshold of ~ 0.2 keV was applied to the central pixel of each event, which has been proven to reduce most of the background due to either the bright Earth limb or the CCD dark current (which depends on the CCD temperature).

The GRBs in our sample were observed with different modes, which were automatically chosen depending on source count rates, to minimize pile-up in the data (Hill et al. 2004). For the GRBs observed during the calibration phase, however, the data were mainly collected in photon counting (PC) mode, and pile-up was often present in the early data. Furthermore, for a few especially bright GRBs (which were observed after the photodiode [PD] mode was discontinued due to a micrometeorite hit on the CCD) the windowed time (WT) data were piled up as well. Generally, WT data were extracted in a rectangular 40 × 20 pixel region centered on the GRB (source region), unless pile-up was present. To account for this effect, the WT data were extracted in a rectangular 40 × 20 pixel region with a region excluded from its center. The size of the exclusion region was determined following the procedures illustrated in Romano et al. (2006a). To account for the background, WT events were also extracted within a rectangular box (40 × 20 pixels) far from background sources.

The PC data were generally extracted from a circular region with a 30 pixel radius. Exceptions were made for bright sources, which required a >30 pixel radius, and for faint sources, which required a smaller radius in order to maintain a high signal-to-noise ratio (S/N). When the PC data suffered from pile-up, we extracted the source events in an annulus with a 30 pixel outer radius and an inner radius depending on the degree of pile-up as determined via the point-spread function (PSF)-fitting method illustrated in Vaughan et al. (2006). PC background data were also extracted in a source-free circular region.

For our analysis we selected XRT grades 0–12 and 0–2 for PC and WT data, respectively (according to *Swift* nomenclature; Burrows et al. 2005a). To calculate the PSF losses, ancillary response files were generated with the task `xrtmkarf` within FTOOLS, and they account for different extraction regions and

TABLE 1
GRB XRT LIGHT-CURVE SAMPLE

GRB Name ^a (1)	Redshift (2)	T_{90} (s) (3)	BAT Fluence ^b (ergs cm ⁻²) (4)	Reference Redshift (5)	Reference BAT (6)	Notes (7)
050406.....	...	5 ± 1	9.0 × 10 ⁻⁸	...	1	XRF
050421.....	...	10.3 ± 2	(1.8 ± 0.7) × 10 ⁻⁷	...	2	
050502B.....	...	17.5 ± 0.2	(8.0 ± 1.0) × 10 ⁻⁷	...	3	
050607.....	...	26.5	(8.9 ± 1.2) × 10 ⁻⁷	...	4	
050712.....	...	48 ± 2	1.8 × 10 ⁻⁶	...	5	
050713A.....	...	70 ± 10	(9.1 ± 0.6) × 10 ⁻⁶	...	6	
050714B.....	...	55.0	(6.5 ± 1.4) × 10 ⁻⁷	...	7	XRF
050716.....	...	69 ± 1	(8.3 ± 1.3) × 10 ⁻⁶	...	8	
050724.....	0.258	3 ± 1	(6.3 ± 1.0) × 10 ⁻⁷	9	10	Short
050726.....	...	30.	(4.3 ± 0.7) × 10 ⁻⁶	...	11	
050730.....	3.967	155 ± 20	(4.4 ± 0.4) × 10 ⁻⁶	12	13	
050801.....	...	20 ± 3	(4.4 ± 1.0) × 10 ⁻⁷	...	14	
050802.....	...	13 ± 2	(2.8 ± 0.3) × 10 ⁻⁶	...	15	
050803.....	0.422	85 ± 10	(3.9 ± 0.3) × 10 ⁻⁶	...	16	
050814.....	...	65 ⁺⁴⁰ ₋₂₀	(2.17 ± 0.36) × 10 ⁻⁶	...	18	
050819.....	...	36 ± 4	(4.2 ± 0.8) × 10 ⁻⁷	...	19	
050820A.....	2.612	26 ± 2	(1.9 ± 0.2) × 10 ⁻⁶	20	21	
050822.....	...	102 ± 2	(3.4 ± 0.3) × 10 ⁻⁶	...	22	
050826 ^e	35 ± 8	(4.3 ± 0.7) × 10 ⁻⁷	...	23	
050904.....	6.29	225 ± 10	(5.4 ± 0.2) × 10 ⁻⁶	...	24	
050908.....	3.3437	20 ± 2	(5.1 ± 0.5) × 10 ⁻⁷	26	27	
050915A.....	...	53 ± 3	(8.8 ± 0.9) × 10 ⁻⁷	...	28	
050916.....	...	90 ± 10	(1.1 ± 0.4) × 10 ⁻⁶	...	29	
050922B.....	...	80 ± 10	(1.8 ± 0.3) × 10 ⁻⁶	...	30	
051016B ^d	0.936	4.0 ± 0.1	(1.7 ± 0.2) × 10 ⁻⁷	31	32	
051117A.....	...	140 ± 10	(4.6 ± 0.16) × 10 ⁻⁶	...	33	
051210.....	...	1.4 ± 0.2	(8.3 ± 1.4) × 10 ⁻⁸	...	34	Short
051227.....	...	8.0 ± 0.2	(2.3 ± 0.3) × 10 ⁻⁷	...	35	
060108.....	...	14.4 ± 1	(3.7 ± 0.4) × 10 ⁻⁷	...	36	
060109 ^e	116 ± 3	(6.4 ± 1.0) × 10 ⁻⁷	...	37	
060111A.....	...	13 ± 1	(1.18 ± 0.05) × 10 ⁻⁶	...	38	
060115.....	3.53	142 ± 5	(1.8 ± 0.2) × 10 ⁻⁶	39	40	
060124 ^f	2.296	321 ± 2	(1.40 ± 0.03) × 10 ⁻⁵	41	42	

^a GRBs with number in italic were considered for their behavior, but did not offer sufficiently high statistics to allow full analysis (see § 2).

^b Drawn from refined BAT GCN Circulars in the 15–150 keV band.

^c A low-signal late-time flare is observed and no analysis was performed.

^d A flattening in the XRT light curve is observed starting from $t \sim 200$ s and lasting through the first SAA data gap. A fit with a Gaussian centered at $t \sim 650$ s provides a significantly worse fit than a combination of power laws; hence, this event was not included in the restricted sample.

^e A flattening in the XRT light curve is observed starting from $t \sim 10^3$ s and lasting through the first SAA data gap.

^f As reported in Romano et al. (2006a) a separate fit was performed to the prompt and the afterglow parts of the X-ray light curve. Here we do not consider the spikes in the prompt.

REFERENCES.—(1) Krimm et al. 2005b; (2) Sakamoto et al. 2005a; (3) Cummings et al. 2005b; (4) Retter et al. 2005; (5) Markwardt et al. 2005a; (6) Palmer et al. 2005c; (7) Tueller et al. 2005a; (8) Barthelmy et al. 2005b; (9) Prochaska et al. 2005b; (10) Krimm et al. 2005a; (11) Barthelmy et al. 2005d; (12) Chen et al. 2005; (13) Markwardt et al. 2005c; (14) Sakamoto et al. 2005c; (15) Palmer et al. 2005a; (16) Bloom et al. 2005; (17) Parsons et al. 2005; (18) Tueller et al. 2005b; (19) Barthelmy et al. 2005c; (20) Prochaska et al. 2005a; (21) Cummings et al. 2005a; (22) Hullinger et al. 2005a; (23) Markwardt et al. 2005b; (24) Haislip et al. 2006; (25) Sakamoto et al. 2005b; (26) Fugazza et al. 2005; (27) Sato et al. 2005b; (28) Barthelmy et al. 2005a; (29) Fenimore et al. 2005; (30) Hullinger et al. 2005c; (31) Soderberg et al. 2005; (32) Barbier et al. 2005; (33) Palmer et al. 2005b; (34) Sato et al. 2005a; (35) Hullinger et al. 2005b; (36) Sakamoto et al. 2006; (37) Palmer et al. 2006; (38) Sato et al. 2006; (39) Piranomonte et al. 2006; (40) Barbier et al. 2006; (41) Mirabal & Halpern 2006; (42) Romano et al. 2006a.

PSF corrections. We used the latest spectral redistribution matrices in the Calibration Database maintained by HEASARC.

From both WT and PC data, light curves were created in the 0.2–10 keV energy band using a criterion of a minimum of 20 source counts per bin and a dynamical subtraction of the background. Therefore, in our sample each light curve was background-subtracted, and corrected for pile-up, vignetting, exposure, and PSF losses.

4. DATA ANALYSIS

The first goal of this work was to obtain a quantitative assessment of flare characteristics. We thus set to measure statistical

parameters such as the ratio of the flare duration to the time of occurrence $\Delta t/t$, the power-law decay slope α_{fall} , the decay to rise ratio $\Delta t_{\text{fall}}/\Delta t_{\text{rise}}$, the flare energetics, and the flare to burst flux ratio. Different approaches suited the data best, depending on the flare statistics, as we outline below.

4.1. $\Delta t/t$ from Gaussian Fits

The simplest analytical characterization of the flare morphology is obtained by adopting a multiply broken power law to model the underlying continuum and a number of Gaussians to model the superposed flares. We adopted the following laws for the continuum: (1) simple power law: $F(t) = Kt^{-\alpha_1}$; (2) broken power

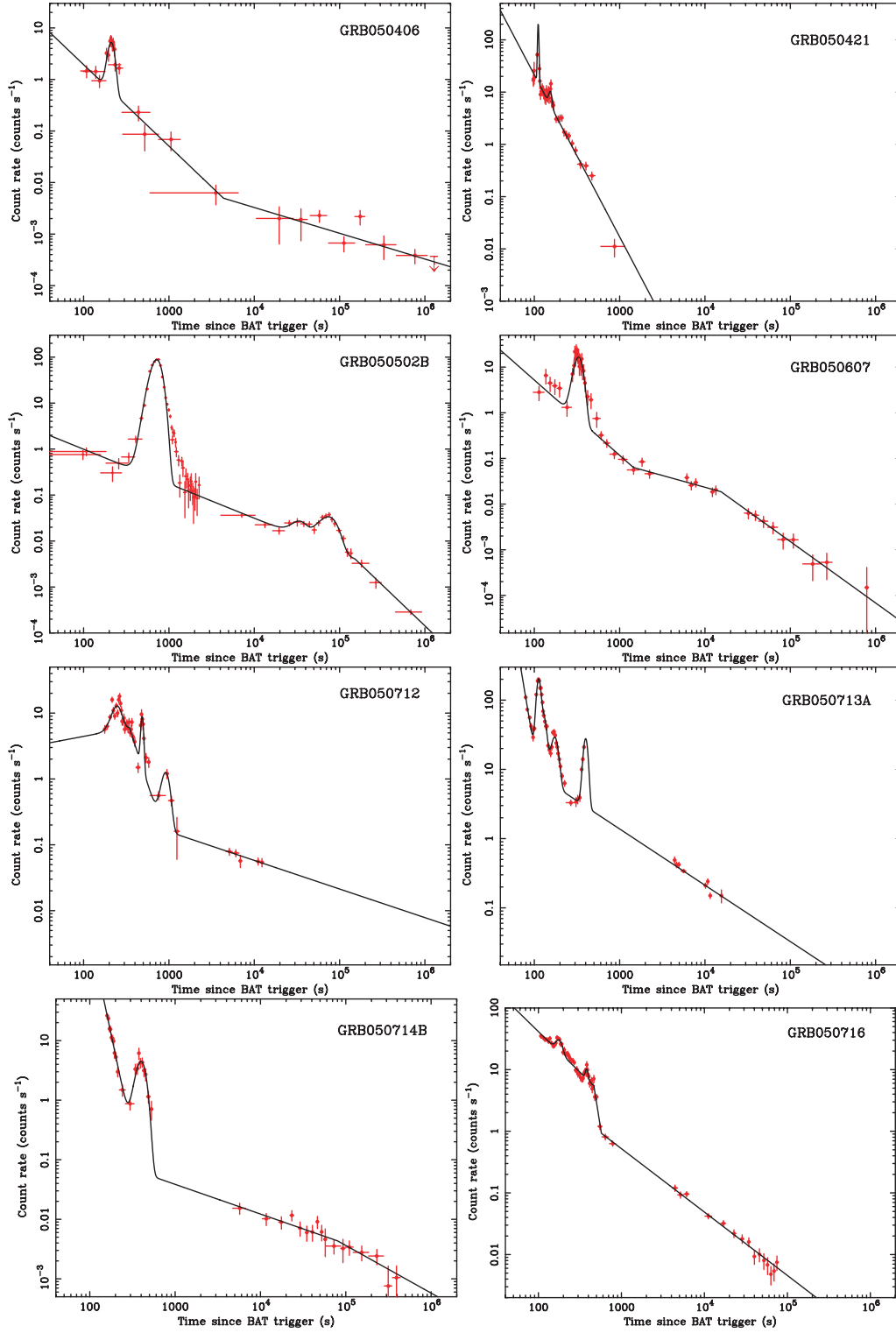


FIG. 1.—Flare fits. The thick line is the best fit to the XRT data (*filled circles*) with a (multiply) broken power law plus a number of Gaussians (see Table 3 for the fit parameters). The continuum and Gaussian parameters are reported in Tables 2 and 3, respectively. For GRB 060124 we considered the prompt and afterglow portion of the light curve separately.

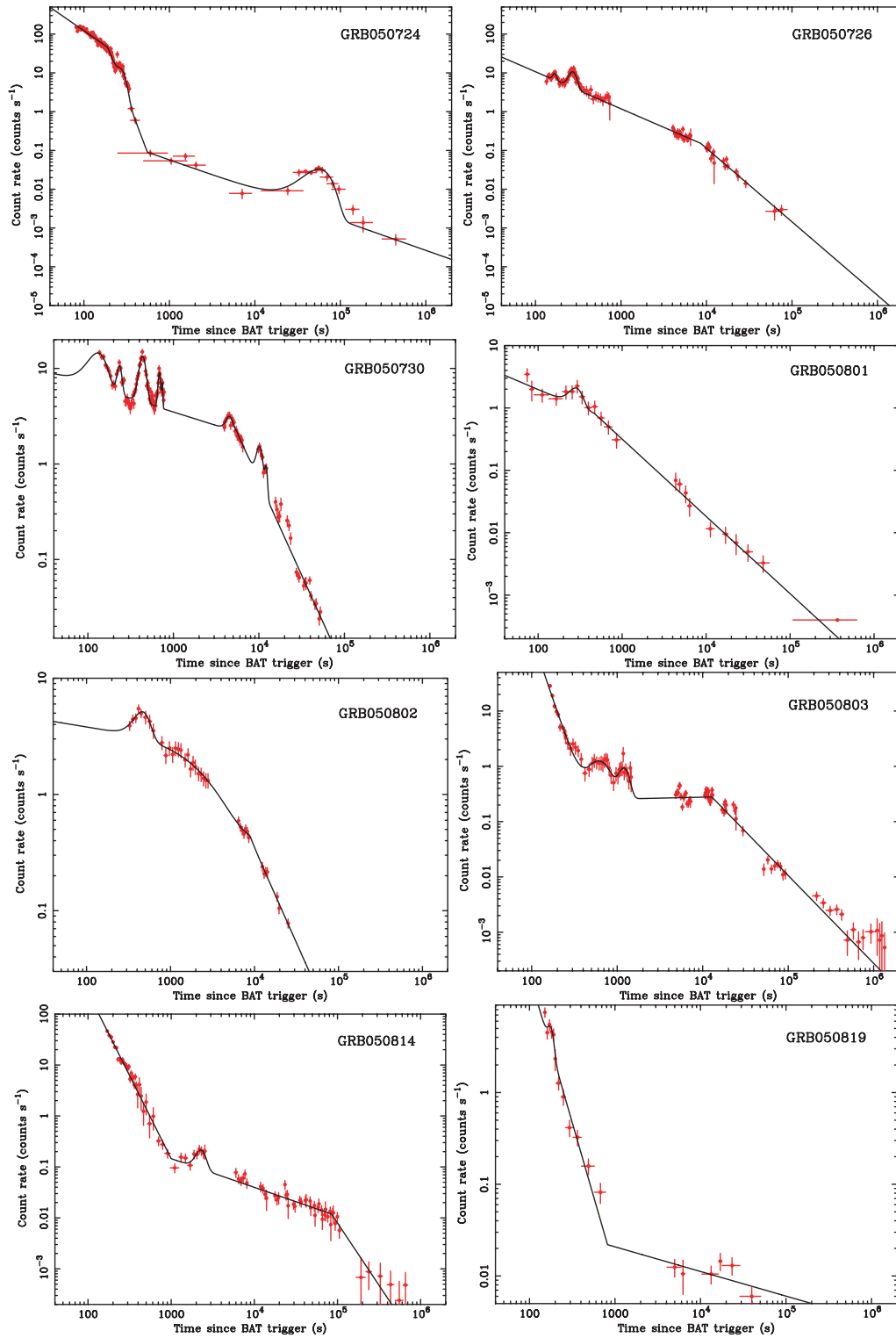


FIG. 1—Continued

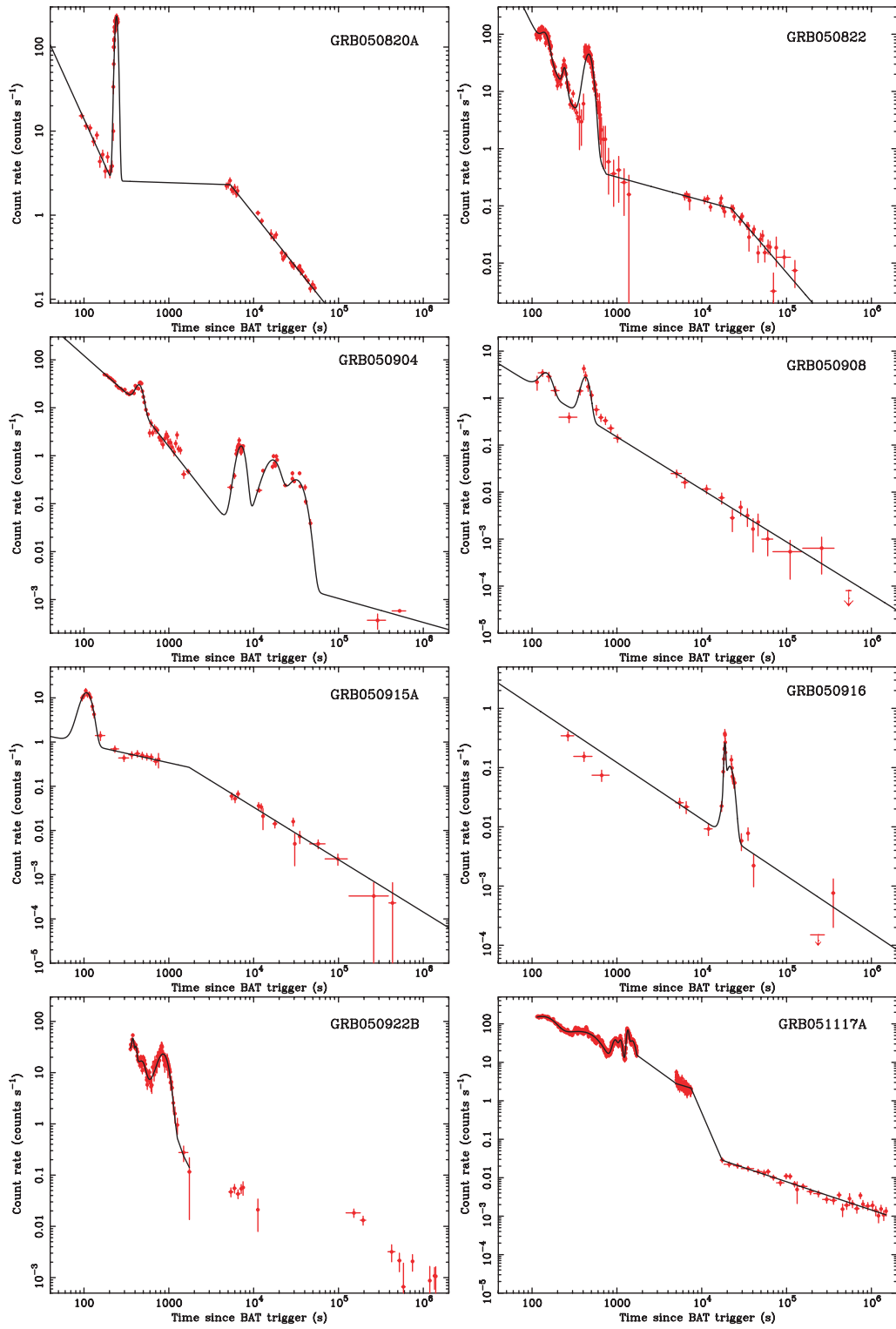


FIG. 1—Continued

TABLE 3—Continued

GRB	Center (s)	Gaussian Width (s)	Norm (counts s ⁻¹)	$\Delta F/F$	EW (s)	α_{fall}	τ_{90} (s)	$\Delta t_{\text{fall}}/\Delta t_{\text{rise}}$	$\Delta t/t^a$
(1)	(2)	(3)	(4)	(5)	(6)	(7)	(8)	(9)	(10)
051227.....	124.2	10.5	5.15	0.88	...	2.05 ± 0.5
060108.....	304^{+24}_{-25}	44^{+130}_{-31}	$0.3^{+0.18}_{-0.12}$	1.83	25
060111A.....	95^{+1}_{-2}	$22.8^{+2.1}_{-1.7}$	$67.6^{+2.7}_{-2.8}$	165.51	73	3.53 ± 0.39	144.4	0.800	1.405
	167^{+1}_{-2}	$18.4^{+2.0}_{-1.8}$	$34.7^{+2.1}_{-2.2}$	7.78	54	4.5 ± 1.2	120.7	1.230	0.719
	280^{+1}_{-2}	$20.6^{+1.7}_{-1.8}$	$85.0^{+4.6}_{-5.2}$	2.11	931	6.51 ± 0.4	177.5	2.430	0.620
060115.....	432^{+19}_{-19}	80^{+26}_{-24}	$1.91^{+0.54}_{-0.45}$	2.53	144.2

^a Using $\Delta t = \tau_{90}$ (the time defined in terms of $f = 0.05$; § 4.3) and $t = t_{\text{peak}}$.

^b GRB 050712 and GRB 050908 have a first flare that quite likely is part of the prompt emission. In addition the decay does not show a very high statistics.

$\Delta t_{\text{fall}}/\Delta t_{\text{rise}}$, $\Delta t/t$ (cols. [8]–[10]), while Figure 7 shows the distributions of $\Delta t_{\text{fall}}/\Delta t_{\text{rise}}$.

4.4. Selection Effects

As stated above, our ability to measure statistical quantities from the light curves critically depends on both the discrete sampling of the light curves and the actual intensity of the flares with respect to the continuum beneath them. In this section we present our considerations on the biases that may affect our analysis and their effect on our results. One of the first difficulties comes from the blending of flares, which causes the EW, Δt , and $\Delta t/t$ to be overestimated. Our result of low $\Delta t/t$ is thus an upper limit on the intrinsic sharpness of flares.

4.4.1. Time Resolution and Low-Earth Orbit Biases

The time resolution of our observations, which decreases logarithmically during the XRT afterglow follow-up, is the first critical factor. Typically, at the beginning of the XRT light curve the sampling is quite good, but if the flare duration is of the order of the time it takes it to fade, then it will not be possible to recognize it as such, and it will be interpreted as a steep power law instead. This was often observed in the early XRT light curves, as reported by Tagliaferri et al. (2005) and O’Brien et al. (2006), and it is partially related to the short but significant time (usually > 60 s) it takes *Swift* to repoint to the GRB. On the other hand, at the end of the XRT light curve, the sampling also degrades because of the long integration required to achieve sufficient S/N, so that flares shorter than the integration time are smeared out, and con-

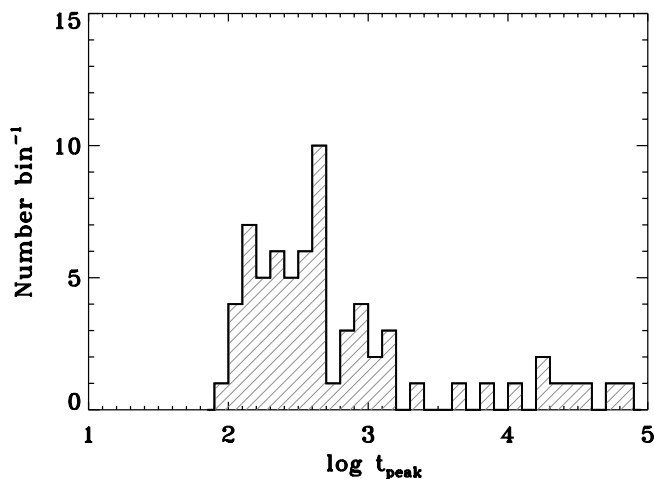


FIG. 2.—Distribution of the peak times of the flares in excess of the canonical XRT light curve. The times are referred to the trigger time and are not corrected for redshift. [See the electronic edition of the Journal for a color version of this figure.]

sequently, except for the brightest ones, their resulting average count rate drops below the detection threshold.

Due to *Swift*'s low-earth orbit, the data are not collected in a continuous way but in portions of an orbit that last less than an hour. This is illustrated in Figure 8 (left), which represents the distribution of the observing times relative to the BAT trigger of all the light curves in our sample. For each observation of the light curve, we estimated the time, which we refer to as bin time (BT), within which the counts were accumulated in order to have a S/N > 3 . For $t > 10^4$ s the BT will generally include data from consecutive orbits. In Figure 8 (right) we show the time resolution (BT) as a function of the time since the BAT trigger, as well as the curve that corresponds to $BT/t = 0.1$ and lies above the large majority of the data. It indicates that the instrumental resolution $BT/t = (\Delta t/t)_{S/N=3}$ is in most cases significantly better than $\Delta t/t \approx 0.1$ and is often even better than 0.01. In other words, our data are not biased against $\Delta t/t \lesssim 0.1$.

4.4.2. Biases in the Sample Definition Criteria

In order to evaluate the completeness of our sample we tested the sample definition criteria against selection effects by means of simulations. First of all, for each flare in our sample, we evaluated S/N as the ratio between the fluence of the flare and the continuum calculated in the time interval $[-1\sigma, +1\sigma]$, where σ is the Gaussian width. The minimum detected S/N is 5. Then, to simulate our procedure, we first calculated the median continuum light curve from the whole data sample. This median light curve

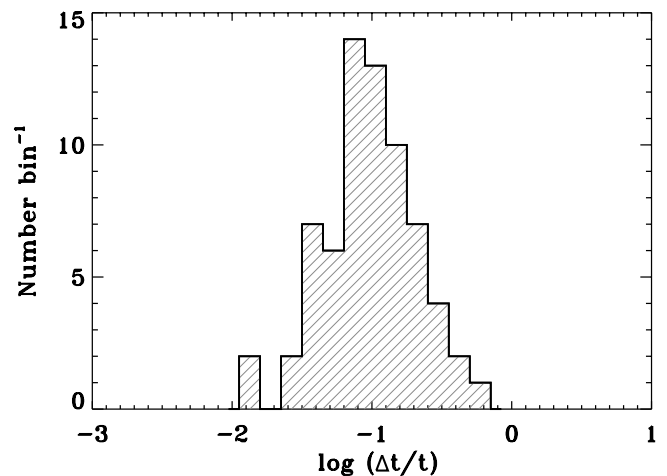


FIG. 3.—Distribution of the ratio of the flare duration vs. the time of occurrence $\Delta t/t$, obtained fitting the flares with Gaussian models (§ 4.1), where Δt is the width of the Gaussian and t is the Gaussian peak time. This ratio is independent of redshift. [See the electronic edition of the Journal for a color version of this figure.]

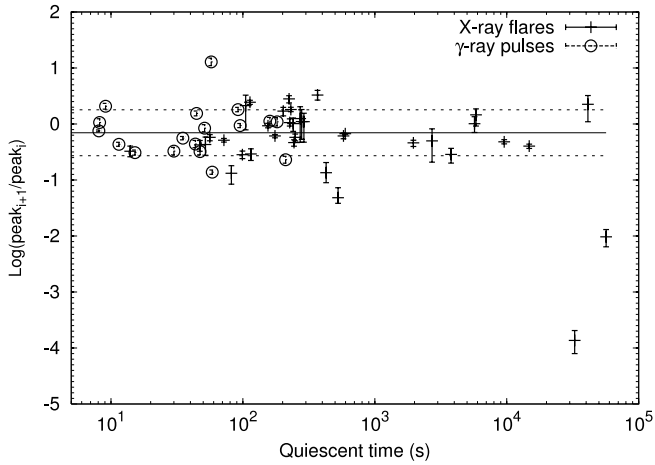


FIG. 11.—Ratio between the peaks of two successive events for both X-ray flares (crosses) and gamma-ray pulses (circles), as a function of the quiescent time between the two events. The solid line shows the mean value, -0.157 , when the two points with the lowest ratio are ignored; dashed lines show the $\pm 1 \sigma$ region. The outliers are GRB 050724 ($\log \text{peak}_{i+1}/\text{peak}_i \sim 10^{-2}$) and GRB 050502B ($\log \text{peak}_{i+1}/\text{peak}_i \sim 10^{-4}$).

accurate description, in many instances an exponential rise followed by a power-law decay or power-law rise followed by a power-law decay is required to produce good fits.

2. Flares are observed in all kinds of GRBs: long (32 GRBs) and short (2 GRBs), high-energy-peaked or XRFs (32 vs. 2); they are found both in early and in late XRT light curves.

3. The equivalent widths of our sample, which measure the flare fluence in terms of the underlying continuum, range between 8 and 7 ; 10^5 s.

4. The distribution of the ratio $\Delta t/t$, as defined by the width and peak of the Gaussians flare models, yields $\langle \Delta t/t \rangle = 0.13 \pm 0.10$. Our simulations show that our time resolution allows us to sample flares that may have $\Delta t/t < 0.1$, so that the above values are not the result of the biases in our sample or our fitting procedures. Our simulations also show that there are no sharp (small $\Delta t/t$) flares at large times.

5. The decay slopes α_{fall} range between 1.3 and 6.8, and generally agree with the curvature effect.

6. The ratios of decay and rise times range between 0.5 and 8.

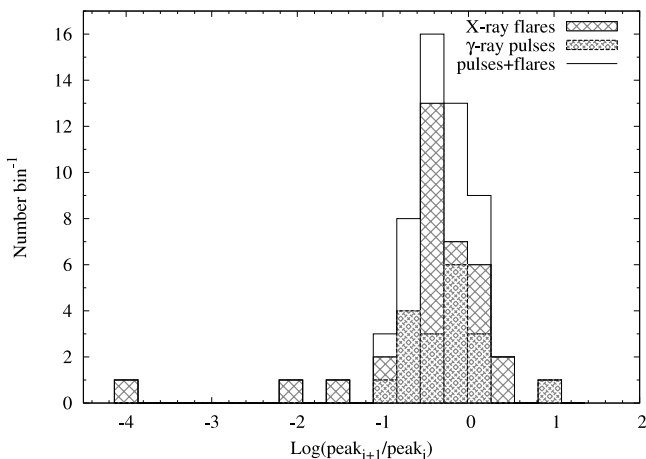


FIG. 12.—Distribution of the ratio between the peaks of two successive events: X-ray flares (cross-hatched), gamma-ray pulses (shaded), both classes (open). [See the electronic edition of the Journal for a color version of this figure.]

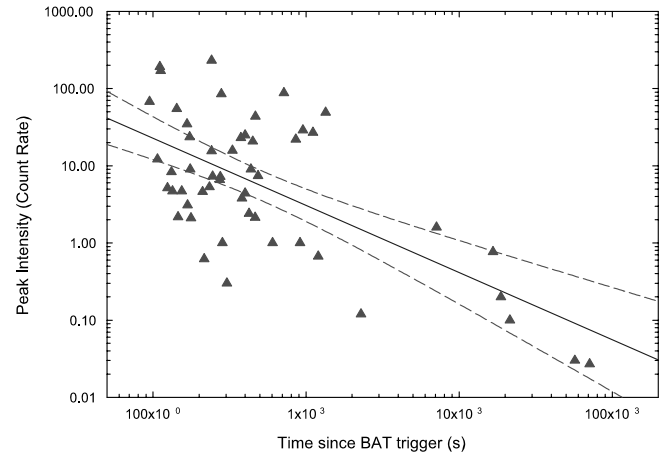


FIG. 13.—Gaussian peaks of the flares as a function of time. The solid line is the best fit, while the dashed lines correspond to 95% confidence limits. [See the electronic edition of the Journal for a color version of this figure.]

7. Correlations are found between

- t_{peak} and peak intensity (strong);
- EW and t_{peak} (very strong);
- α_{fall} and t (poor);
- $\Delta t_{\text{fall}}/\Delta t_{\text{rise}}$ and τ_{90} (tentative).

8. We do not find any clear correlation between the number of gamma-ray pulses and the number of X-ray flares. One cannot infer anything about the number of X-ray flares from the number of gamma-ray pulses and vice versa. We also conclude that the relation between successive pulses and between successive flares is the same: in particular, on average the next event has a peak $10^{-0.157} \simeq 0.7$ times as high as the preceding, while the scatter is between 0.3 and 1.8. This is a piece of evidence pointing to a common origin for gamma-ray pulses and X-ray flares.

7. DISCUSSION

The analysis of the flares in the present sample, together with the revisiting of the canonical XRT light curve (Chincarini et al. 2005; Nousek et al. 2006; O'Brien et al. 2006; Zhang et al. 2006), makes it clear that the onset of the XRT observation corresponds to the late tail of the prompt emission as defined in the current model. Flares are often observed in the early XRT light curves. Their slopes do not conflict with the curvature effect limit; they simply need a different interpretation and a proper location of T_0 (Liang et al. 2006).

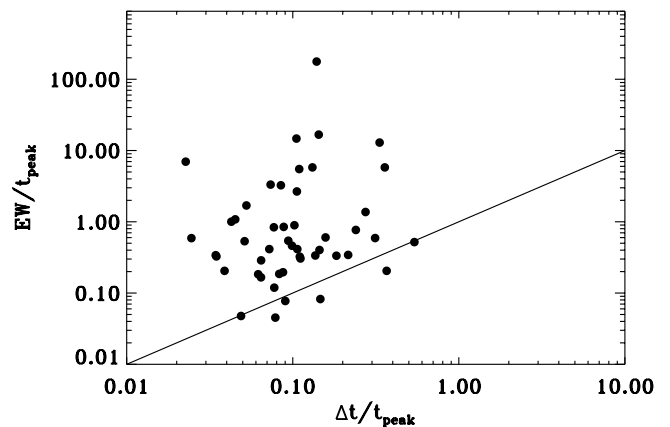


FIG. 14.—EW/ t_{peak} vs. $\Delta t/t_{\text{peak}}$. The solid line is the bisector of the plane.

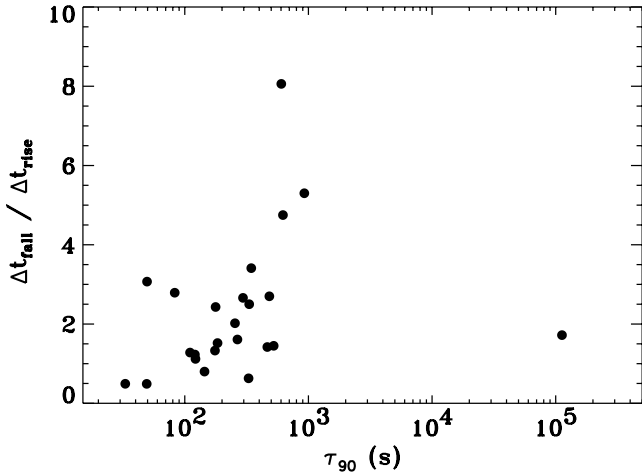


FIG. 15.— $\Delta t_{\text{fall}}/\Delta t_{\text{rise}}$ vs. τ_{90} .

Similar reasoning explains the decay slope of the flares. We have seen, in agreement with the finding of Liang et al. (2006), that the decay slope is very sensitive to the definition of T_0 and that if this is located at the beginning of the flares, we are within the constraint of the curvature effect. This essentially means that the shock, after reaching the maximum luminosity, is not fed anymore and fades out. Some of the uncertain or critical cases of flares may be due to the presence of blends. Blends and superposed miniflares are indeed very common, and we can observe them very clearly in all those cases in which the statistics are very good. Although the analysis may be affected in part by this contamination, the results remain robust. Indeed, the contamination makes our results even more robust, since the detection of unseen blends would make the selected T_0 large, thus decreasing the measured slope and width of the flares.

We also considered the possibility of a correlation between the characteristics of the prompt emission as observed by BAT and the frequency of flares detected by XRT. We found no correlation. This simply means that the flares are random events and are not related to the way the prompt emission develops in time. For instance, there could be an initial flickering, due to the collision of highly relativistic shells followed by random flare events due to the collision of slower residual pellets, as discussed below. The contamination to our sample due to the fact that some of the early XRT flares are the tail of the late prompt emission does not change this result. However, this needs to be further investigated using a larger statistical sample.

Furthermore, we have shown that our analysis is not affected by bias in the detection of high-intensity late flares and that such flares never show a peak of intensity as strong as those observed in the early flares. On the other hand, due to their rather long duration, these flares are also very energetic.

Most of the indications we have so far seem to lead toward an activity that is very similar to that of the prompt emission, with flares that are superposed on a very standard light curve. This has been observed both in long and short bursts.

In light of the calculations of Ioka et al. (2005) we calculated $\Delta F/F$ and $\Delta t/t$ values from our flare sample and plotted them over the kinematically allowed regions for afterglow variabilities, as shown in Figure 16. Ioka et al. (2005) distinguish between four cases: (1) dips, arising from nonuniformity on the emitting surface induced, e.g., by density fluctuations (eq. [4] in Ioka et al. 2005); (2) bumps due to density fluctuations (Wang & Loeb 2000; Lazzati et al. 2002; Dai & Lu 2002) (eq. [7] in Ioka et al. 2005); (3) bumps

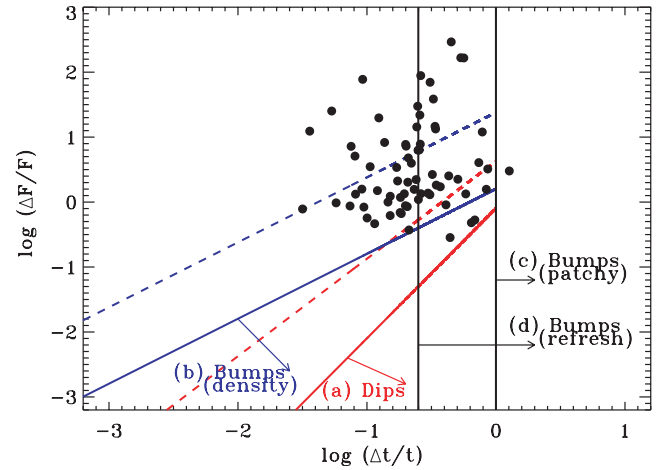


FIG. 16.—Scatter plot of $\Delta F/F - \Delta t/t$ values calculated on our flare samples on the kinematically allowed regions for afterglow variabilities according to Ioka et al. (2005). Data are drawn from Tables 2 and 3. We used the FWHM of the Gaussians as Δt , the Gaussian peak time for t , while the ratio of the peak flux over the underlying continuum flux ($\Delta F/F$) was calculated using the best-fit models. The four limits plotted are based on (a) eq. (4) in Ioka et al. (2005) for dips (shown on axis), (b) eq. (7) in Ioka et al. (2005) for bumps due to density fluctuations (on axis), (c) $\Delta t > t$ for bumps due to patchy shells, and (d) $\Delta t > t/4$ for bumps due to refreshed shocks. According to Ioka et al. (2005) when many regions fluctuate simultaneously, limits *a* and *b* are replaced by eqs. (A1) and (A2) in Ioka et al. (2005), respectively. The off-axis cases (viewing angle $\theta_v \sim \gamma^{-1}/2 \gtrsim \Delta\theta$, where $\Delta\theta$ is the half-angular size of the variable region) are shown by dashed lines.

due to patchy shells (Mészáros et al. 1998; Kumar & Piran 2000a), for which $\Delta t > t$; (4) bumps due to refreshed shocks (Rees & Mészáros 1998; Panaitescu et al. 1998; Kumar & Piran 2000b), for which $\Delta t > t/4$.

Our findings are consistent with the conclusion of Zhang et al. (2006) and Lazzati & Perna (2007), the latter based on a preliminary presentation of our data set in Chincarini (2007); i.e., a sizable fraction of the flares cannot be related to the external shock mechanisms.⁹

In particular, only one point (corresponding to a flare in GRB 051117A) lies in the region of $\Delta t > t$, where flares are consistent with the patchy shells model. Only three points (including the early flare of GRB 050502B) lie in the region of flares that can be caused by ambient density fluctuations. Only 29/69 points lie in the region that describes flares due to refreshed shocks, although we note that in a few specific cases, e.g., GRB 050713A (Guetta et al. 2007) and GRB 050730 (Perri et al. 2007), the refreshed-shock model is preferred. Finally, among the rest, 10/69 can only be due to internal shocks.

Perna et al. (2006) proposed that X-ray flares are due to accretion of a fragmented disk. Due to viscous evolution, blobs far from the central black hole take longer to be accreted and are therefore more spread out when accretion occurs. The accretion rate is correspondingly lower. This naturally gives a peak luminosity–flare epoch anticorrelation, as has been revealed by the data. This same merit could be retained if a magnetic barrier

⁹ We note that recently Dermer (2007) argued that strong X-ray flares may be also reproduced within the external shock model if the blast wave is assumed to sweep density clouds with an angular extension less than the relativistic beaming angle $1/\Gamma$. The simulated light curves in the logarithmic space are, however, generally broad with a wide, flat peak, in contrast to the observed sharply peaking flare light curves. It is also not straightforward within the model to explain the “coincidence” of T_0 at the beginnings of many flares (Liang et al. 2006), which is naturally accounted for within the internal emission model by assuming that the rapid decay following the peak is due to the curvature effect.

modulates a continuous accretion flow near the black hole at different epochs (Proga & Zhang 2006).

This work is supported at the Osservatorio Astronomico di Brera by ASI grant I/R/039/04, at Penn State by NASA contract NAS5-

00136, and at the University of Leicester by PPARC. We gratefully acknowledge the contributions of dozens of members of the XRT and BAT teams at OAB, PSU, UL, GSFC, ASDC, and MSSL and our subcontractors, who helped make these instruments possible.

Facilities: Swift

REFERENCES

- Band, D., et al. 1993, *ApJ*, 413, 281
- Barbier, L., et al. 2006, *GCN Circ.*, 4518, <http://gcn.gsfc.nasa.gov/gcn3/4518.gcn3>
- . 2005, *GCN Circ.*, 4104, <http://gcn.gsfc.nasa.gov/gcn3/4104.gcn3>
- Barthelmy, S., et al. 2005a, *GCN Circ.*, 3982, <http://gcn.gsfc.nasa.gov/gcn3/3982.gcn3>
- . 2005b, *GCN Circ.*, 3629, <http://gcn.gsfc.nasa.gov/gcn3/3629.gcn3>
- . 2005c, *GCN Circ.*, 3828, <http://gcn.gsfc.nasa.gov/gcn3/3828.gcn3>
- . 2005d, *GCN Circ.*, 3682, <http://gcn.gsfc.nasa.gov/gcn3/3682.gcn3>
- Barthelmy, S. D., et al. 2005e, *Space Sci. Rev.*, 120, 143
- . 2005f, *Nature*, 438, 994
- Bloom, J. S., Perley, D., Foley, R., Prochaska, J. X., Chen, H. W., & Starr, D. 2005, *GCN Circ.*, 3758, <http://gcn.gsfc.nasa.gov/gcn3/3758.gcn3>
- Burrows, D. N., et al. 2005a, *Space Sci. Rev.*, 120, 165
- . 2005b, *Science*, 309, 1833
- . 2006, in *The X-Ray Universe 2005*, ed. A. Wilson (ESA SP-604; Noordwijk: ESA), 877
- Campana, S., et al. 2006, *A&A*, 454, 113
- Chen, H.-W., Thompson, I., Prochaska, J. X., & Bloom, J. 2005, *GCN Circ.*, 3709, <http://gcn.gsfc.nasa.gov/gcn3/3709.gcn3>
- Chincarini, G. 2007, in *Frontier Objects in Astrophysics and Particle Physics*, ed. F. Giovannelli & G. Mannocchi (Bologna: Italian Phys. Soc.), in press (astro-ph/0608414)
- Chincarini, G., et al. 2005, *ApJ*, submitted (astro-ph/0506453)
- . 2006, in *The X-Ray Universe 2005*, ed. A. Wilson (ESA SP-604; Noordwijk: ESA), 871
- Cummings, J., et al. 2005a, *GCN Circ.*, 3835, <http://gcn.gsfc.nasa.gov/gcn3/3835.gcn3>
- . 2005b, *GCN Circ.*, 3339, <http://gcn.gsfc.nasa.gov/gcn3/3339.gcn3>
- Cusumano, G., et al. 2006, *Nature*, 440, 164
- Dai, Z. G., & Lu, T. 2002, *ApJ*, 565, L87
- Daigle, F., & Mochkovitch, R. 1998, *MNRAS*, 296, 275
- Dermer, C. D. 2004, *ApJ*, 614, 284
- . 2007, *ApJ*, 664, 384
- Falcone, A. D., et al. 2006, *ApJ*, 641, 1010
- . 2007, *ApJ*, 671, 1921
- Fenimore, E., et al. 2005, *GCN Circ.*, 4003, <http://gcn.gsfc.nasa.gov/gcn3/4003.gcn3>
- Ford, L. A., et al. 1995, *ApJ*, 439, 307
- Fugazza, D., et al. 2005, *GCN Circ.*, 3948, <http://gcn.gsfc.nasa.gov/gcn3/3948.gcn3>
- Gehrels, N., et al. 2004, *ApJ*, 611, 1005
- . 2006, *Nature*, 444, 1044
- Goad, M. R., et al. 2006, *A&A*, 449, 89
- Guetta, D., et al. 2007, *A&A*, 461, 95
- Haislip, J. B., et al. 2006, *Nature*, 440, 181
- Heise, J., in 't Zand, J., Kippen, R. M., & Woods, P. M. 2001, in *Gamma-Ray Bursts in the Afterglow Era*, ed. E. Costa, F. Frontera, & J. Hjorth (New York: Springer), 16
- Hill, J. E., et al. 2004, *Proc. SPIE*, 5165, 217
- Hullinger, D., et al. 2005a, *GCN Circ.*, 3856, <http://gcn.gsfc.nasa.gov/gcn3/3856.gcn3>
- . 2005b, *GCN Circ.*, 4400, <http://gcn.gsfc.nasa.gov/gcn3/4400.gcn3>
- . 2005c, *GCN Circ.*, 4019, <http://gcn.gsfc.nasa.gov/gcn3/4019.gcn3>
- Ioka, K., Kobayashi, S., & Zhang, B. 2005, *ApJ*, 631, 429
- Kobayashi, S., Zhang, B., Mészáros, P., & Burrows, D. 2007, *ApJ*, 655, 391
- Krimm, H., et al. 2005a, *GCN Circ.*, 3667, <http://gcn.gsfc.nasa.gov/gcn3/3667.gcn3>
- . 2005b, *GCN Circ.*, 3183, <http://gcn.gsfc.nasa.gov/gcn3/3183.gcn3>
- Kumar, P., & Panaitescu, A. 2000, *ApJ*, 541, L51
- Kumar, P., & Piran, T. 2000a, *ApJ*, 535, 152
- . 2000b, *ApJ*, 532, 286
- Lazzati, D., & Perna, R. 2007, *MNRAS*, 375, L46
- Lazzati, D., Rossi, E., Covino, S., Ghisellini, G., & Malesani, D. 2002, *A&A*, 396, L5
- Li, H., & Fenimore, E. E. 1996, *ApJ*, 469, L115
- Liang, E. W., et al. 2006, *ApJ*, 646, 351
- Markwardt, C., et al. 2005a, *GCN Circ.*, 3576, <http://gcn.gsfc.nasa.gov/gcn3/3576.gcn3>
- . 2005b, *GCN Circ.*, 3888, <http://gcn.gsfc.nasa.gov/gcn3/3888.gcn3>
- Markwardt, C. B., et al. 2005c, *GCN Circ.*, 3715, <http://gcn.gsfc.nasa.gov/gcn3/3715.gcn3>
- Mészáros, P., Rees, M. J., & Wijers, R. A. M. J. 1998, *ApJ*, 499, 301
- Mirabal, N., & Halpern, J. P. 2006, *GCN Circ.*, 4591, <http://gcn.gsfc.nasa.gov/gcn3/4591.gcn3>
- Norris, J. P., Nemiroff, R. J., Bonnell, J. T., Scargle, J. D., Kouveliotou, C., Paciesas, W. S., Meegan, C. A., & Fishman, G. J. 1996, *ApJ*, 459, 393
- Nousek, J. A., et al. 2006, *ApJ*, 642, 389
- O'Brien, P. T., et al. 2006, *ApJ*, 647, 1213
- Pagani, C., et al. 2006, *ApJ*, 645, 1315
- Palmer, D., et al. 2005a, *GCN Circ.*, 3737, <http://gcn.gsfc.nasa.gov/gcn3/3737.gcn3>
- . 2005b, *GCN Circ.*, 4289, <http://gcn.gsfc.nasa.gov/gcn3/4289.gcn3>
- . 2005c, *GCN Circ.*, 3597, <http://gcn.gsfc.nasa.gov/gcn3/3597.gcn3>
- . 2006, *GCN Circ.*, 4476, <http://gcn.gsfc.nasa.gov/gcn3/4476.gcn3>
- Panaitescu, A., Mészáros, P., & Rees, M. J. 1998, *ApJ*, 503, 314
- Parsons, A., et al. 2005, *GCN Circ.*, 3757, <http://gcn.gsfc.nasa.gov/gcn3/3757.gcn3>
- Perna, R., Armitage, P. J., & Zhang, B. 2006, *ApJ*, 636, L29
- Perri, M., et al. 2007, *A&A*, 471, 83
- Piranomonte, S., et al. 2006, *GCN Circ.*, 4520, <http://gcn.gsfc.nasa.gov/gcn3/4520.gcn3>
- Piro, L., et al. 1999, *ApJ*, 514, L73
- . 2005, *ApJ*, 623, 314
- Prochaska, J. X., Bloom, J. S., Wright, J. T., Butler, R. P., Chen, H. W., Vogt, S. S., & Marcy, G. W. 2005a, *GCN Circ.*, 3833, <http://gcn.gsfc.nasa.gov/gcn3/3833.gcn3>
- Prochaska, J. X., Chen, H.-W., Bloom, J. S., & Stephens, A. 2005b, *GCN Circ.*, 3679, <http://gcn.gsfc.nasa.gov/gcn3/3679.gcn3>
- Proga, D., & Zhang, B. 2006, *MNRAS*, 370, L61
- Rees, M. J., & Mészáros, P. 1998, *ApJ*, 496, L1
- Retter, A., et al. 2005, *GCN Circ.*, 3525, <http://gcn.gsfc.nasa.gov/gcn3/3525.gcn3>
- Romano, P., et al. 2006a, *A&A*, 456, 917
- . 2006b, *A&A*, 450, 59
- Sakamoto, T., et al. 2006, *GCN Circ.*, 4445, <http://gcn.gsfc.nasa.gov/gcn3/4445.gcn3>
- . 2005a, *GCN Circ.*, 3305, <http://gcn.gsfc.nasa.gov/gcn3/3305.gcn3>
- . 2005b, *GCN Circ.*, 3938, <http://gcn.gsfc.nasa.gov/gcn3/3938.gcn3>
- . 2005c, *GCN Circ.*, 3730, <http://gcn.gsfc.nasa.gov/gcn3/3730.gcn3>
- Sato, G., et al. 2005a, *GCN Circ.*, 4318, <http://gcn.gsfc.nasa.gov/gcn3/4318.gcn3>
- . 2005b, *GCN Circ.*, 3951, <http://gcn.gsfc.nasa.gov/gcn3/3951.gcn3>
- . 2006, *GCN Circ.*, 4486, <http://gcn.gsfc.nasa.gov/gcn3/4486.gcn3>
- Soderberg, A. M., Berger, E., & Ofek, E. 2005, *GCN Circ.*, 4186, <http://gcn.gsfc.nasa.gov/gcn3/4186.gcn3>
- Tagliaferri, G., et al. 2005, *Nature*, 436, 985
- Tueller, J., et al. 2005a, *GCN Circ.*, 3615, <http://gcn.gsfc.nasa.gov/gcn3/3615.gcn3>
- . 2005b, *GCN Circ.*, 3803, <http://gcn.gsfc.nasa.gov/gcn3/3803.gcn3>
- Vaughan, S., et al. 2006, *ApJ*, 638, 920
- Wang, X., & Loeb, A. 2000, *ApJ*, 535, 788
- Zhang, B., Fan, Y. Z., Dyks, J., Kobayashi, S., Mészáros, P., Burrows, D. N., Nousek, J. A., & Gehrels, N. 2006, *ApJ*, 642, 354

